Multi-Band Miniaturized Antenna Loaded by ZOR and CSRR Metamaterial Structures With Monopolar Radiation Pattern

Aidin Mehdipour, *Member, IEEE*, Tayeb A. Denidni, *Senior Member, IEEE*, and Abdel-Razik Sebak, *Fellow, IEEE*

***Abstract*—Miniaturized low-profile monopole antennas loaded by metamaterial (MTM) structures are presented. The antenna is loaded by zeroth-order resonator (ZOR) and complimentary split-ring resonator (CSSR) units, resonating over three frequency bands so that they can be tuned by changing the geometrical parameters of the MTM structures. Surface current distribution and equivalent circuit models are provided to describe the principle of operation. The experimental results are presented to validate the numerical results. Showing the monopole-shape radiation pattern characteristics at all resonant frequencies, the proposed MTM antennas are suitable for vehicular wireless applications.**

***Index Terms*—Antenna miniaturization, artificial materials, complimentary split ring resonator (CSRR), metamaterials, monopolar radiation pattern, multiband antennas, vehicular applications.**

I. Introduction

RECENTLY, vehicular communication systems have been extensively developed in many industrial and military applications for public safety, navigation, security, surveillance, telemetry, and environment monitoring issues [1], [2]. In these systems, vehicular sensor networks (VSNs) are used as mobile sensor platforms to collect necessary data and exchange information with other mobile or stationary communication devices or base stations. For example, Intelligent Transportation Systems (ITS) have increasingly employed VSNs for traffic and weather data collection, incident detection, hazardous vehicle identification, intelligent speed adaptation, and alert/warning information [2]. The vehicular networks use various wireless communication methods such as cellular networks and Universal Mobile Telecommunication Systems (UMTS) (1750–1780, 2010–2025, 2110–2170, 2620–2690 MHz), Personal Communication Systems (PCS) (1670–1675 MHz, 1910–1915, 1990–1995), General Wireless Communication Service (GWCS) (2305–2320, 2345–2360, 4660–4685, 4940–4990 MHz), Bluetooth, WiFi and WiMax (2446–2456, 3500–3505 MHz), and Dedicated Short Range Communication (DSRC) (Europe: 2010–2020, 5795–5805, 5875–5905 MHz, North America: 5850–5925 MHz) [1]–[10]. Note that vehicular networks are basically narrowband especially when fast and reliable communication is demanded. For example, for DSRC applications, the required bandwidth is only 10 MHz at 2 GHz, and 10 to 30 MHz at 5 GHz in Europe, and 75 MHz at 5 GHz in North America [5]. For public safety applications, the bandwidth is 50 MHz at 4.9 GHz carrier frequency [10].

In vehicular applications, transmitters and receivers are predominantly located and communicating in the horizontal plane so that the radiation pattern of the antennas should be very weak at broadside direction, but strong and omni-directional at lower elevation angles [5]–[8]. Due to their conical radiation pattern characteristics, monopole antennas above ground plane are one of the most common and desirable antennas for vehicular communication systems. However, monopole antennas have two major disadvantages, namely a large electrical size which is about $\lambda/4$ and only a single resonant frequency response which is associated with the fundamental mode [11], [12]. In addition to the compact size, a multi-band frequency response is very suitable and important characteristic for new antennas in emerging wireless communication systems [6], [19]. Moreover, independent tunability of operating frequency bands is a desirable but challenging feature for the antennas.

Due to the interesting and exotic characteristics, metamaterial (MTM) structures have been extensively used to miniaturize the size of the antennas and to obtain multiband frequency response [13]. Providing zero and negative order resonances $(n = 0, -1, -2, \ldots)$, composite right/left handed (CRLH) unit cells are of much interest in MTM antenna design to achieve miniaturization [14]–[20]. However, in most of the work on multiband MTM antennas, the radiation pattern is not monopolar at all resonant frequencies and also independent tunability at different resonant frequencies is challenging so that periodic CRLH structures are often composed of lumped components, namely series capacitors and shunt inductors, which increases the complexity of the design and fabrication. Therefore, periodic CRLH antennas may not be lonely able to address all design requirements for a specific application. Recently, combining CRLH units with other radiating elements has been of much

Manuscript received April 12, 2013; revised November 01, 2013; accepted November 05, 2013. Date of publication November 14, 2013; date of current version January 30, 2014. This work was supported in part by the Natural Sciences and Engineering Research Council of Canada (NSERC).

A. Mehdipour was with the INRS-EMT, Université du Quebec, Montreal, QC H5A 1K6, Canada. He is now with the Edward S. Rogers Sr. Department of Electrical and Computer Engineering, University of Toronto, Toronto, ON M5S 3G4, Canada (e-mail: aidin.mehdipour@utoronto.ca).

T. A. Denidni is with the INRS-EMT, Université du Quebec, Montreal, QC H5A 1K6, Canada (e-mail: denidni@inrs.emt.ca).

A.-R. Sebak is with the Department of Electrical and Computer Engineering, Concordia University, Montreal QC H3G 2W1, Canada (e-mail: abdo@ece.concordia.ca).

Color versions of one or more of the figures in this paper are available online at http://ieeexplore.ieee.org.

Digital Object Identifier 10.1109/TAP.2013.2290791

interest to design MTM-inspired antennas with simple structure and desirable multifunctional characteristics [21], [22].

Recently, split ring resonator (SRR) and complimentary split ring resonator (CSRR) structures have efficiently been used to reduce the antenna size significantly [23]–[30], or to improve the impedance matching [31]. In addition to high level of miniaturization, since the electrical parameters, i.e., capacitance and inductance, of these meta-resonators can be easily tailored by tuning the geometrical dimensions, SRRs and CSRRs have been very attractive for compact antenna designs with adjustable frequency response [25]–[30]. It should be pointed out that due to the high level of miniaturization, using these structures may decrease the radiation efficiency of the antennas significantly. For example, in [28], the radius of circular patch antenna loaded with CSRR is reduced by 75% with the radiation efficiency of 28.1%. In [29], rectangular patch antennas with ground plane loaded by CSRR shows the radiation efficiency between 19 and 25%.

In this paper, we propose miniaturized monopole antenna loaded by MTM structures, namely CRLH mushroom and CSRR units, for vehicular applications. The antenna operates over three tunable resonant frequencies. The monopole is loaded with mushroom units at horizontal plane so that the mushrooms are designed to radiate the electric field of zero order mode. The other tunable resonant frequency can be obtained by etching CSRR unit on the mushrooms surface, which reduces the resonant frequency of rectangular patch. In another design, by changing the location of CSRR units on mushrooms, further miniaturization at the zero order resonance is achieved while other two resonances are maintained. A monopolar radiation pattern is achieved at all frequency bands. In Section II, the antenna geometry and parametric study is presented. The antenna principle of operation and design guideline are explained by calculating the dispersion diagrams and providing an equivalent circuit model of the antenna. Section III contains experimental results validated by simulations. Section IV contains conclusions.

II. Metamaterial Antenna Design

Fig. 1 shows the proposed MTM antenna. The antenna consists of a printed z -directed monopole antenna loaded by a CSRR unit named as CSRR1, and four mushroom units located at *xy* plane loaded by CSRR structures named as CSRR2. The antenna is fed through a 50-ohm SMA connector from below the ground plane. The connector pin is connected to the feed section as shown in Fig. 1(b). The mushrooms are connected through vias to the ground plane. Providing a monopolar radiation pattern, mushroom structures act as magnetic loops when a zero order mode is excited [13]. The substrate of mushroom units is chosen to be RO5880 ($\varepsilon_r = 2.2$) with 1.57 mm of thickness. The printed monopole substrate is RO4003 ($\varepsilon_r = 3.55$) with the thickness of 0.5 mm and the CSRR1 structure is printed on the other side of the substrate as shown in Fig. 1(c). The geometrical parameters of the antenna are given as $\mathrm{R_{CSRR1}} = 4.7, \mathrm{R_{CSRR2}} = 2.6, \mathrm{R_{via}} = 0.2, w_1 = 8, w_2 = 13, d = 4.7, s_1 = s_2 = 0.3, \Delta_1 = \Delta_2 = 0.2$, $L_1 = 18, L_2 = 11, g = 0.2, w = 0.9, h_m = 13$, and $h_s = 16$ mm. Fig. 2 shows the S_{11} parameter of the antenna. All simulations are performed using CST MWS software tool [32]. It is observed that

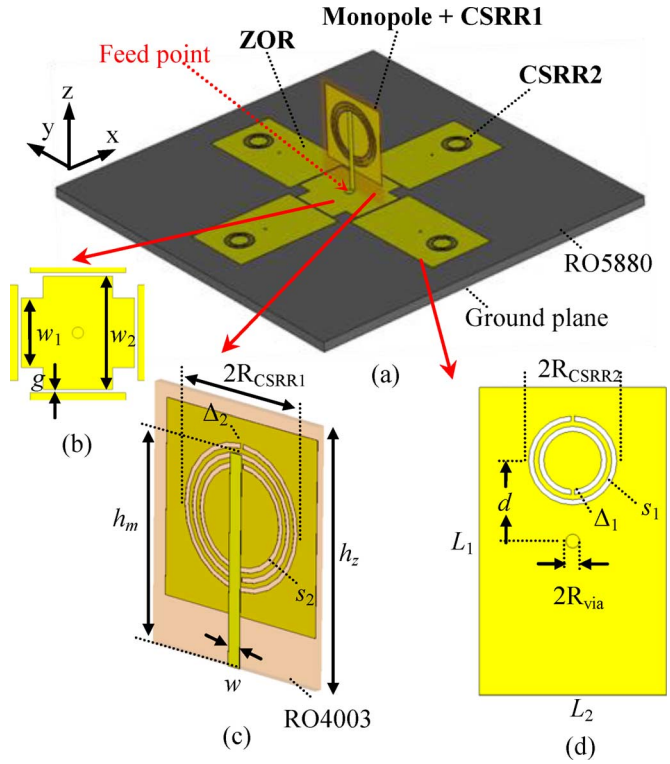

Fig. 1. (a) Proposed MTM antenna, (b) feed section, (c) printed monopole loaded with CSRR1, (d) mushroom ZOR loaded with CSRR2.

the resonant frequencies f_1, f_2, and f_3 can be tuned by changing $\mathrm{R_{CSRR1}}, \mathrm{R_{via}}$, and $\mathrm{R_{CSRR2}}$ parameters, respectively. The parameter g is used to adjust the matching at f_2 and f_3 by controlling the gap capacitance between feed section and mushroom structures. Two weak resonances between 3.5 and 4 GHz frequencies, which are due to the higher order modes of printed monopole loaded by CSRR1, are not of our interest.

Fig. 3(a) shows the strong current distribution of CSRR1 at f_1 frequency. The height of monopole is about $h_z = 0.1\lambda$ which is much smaller than 0.25λ height of conventional monopole. Mushroom units acts as MTM infinite wavelength structure by resonating at f_2, which is the resonant frequency of $n = 0$ mode. In this case, the resonant frequency is independent of the size of the resonator. The electric field and current distribution of one mushroom unit is obtained at f_2 as shown in Fig. 3(b). It is observed that the electric field is in-phase along the patch which is the characteristics of zeroth order resonator (ZOR) structures. Fig. 3(c) shows that the CSRR2 couples the power to the microstrip patch at f_3 frequency so that the $\mathrm{TM_{10}}$ mode with out-of-phase electric field is radiated with lowered resonant frequency. The effect of CSRR2 unit is explained in more detail as displayed in Fig. 4. It is observed that the resonant frequency of 0.25λ wire monopole (Fig. 4(a)) is around 2.1 GHz and by loading the wire monopole with CRLH unit (Fig. 4(b)), the second frequency band is introduced at 3.2 GHz and the third resonant occurs at around 5.2 GHz. However, the resonance at f_3 is not well matched and it cannot be well tuned without affecting f_2 frequency band. By introducing CSRR to mushroom structure, the resonant frequency at f_3 is lowered with good matching and it can also be tuned independently by changing CSRR dimensions.

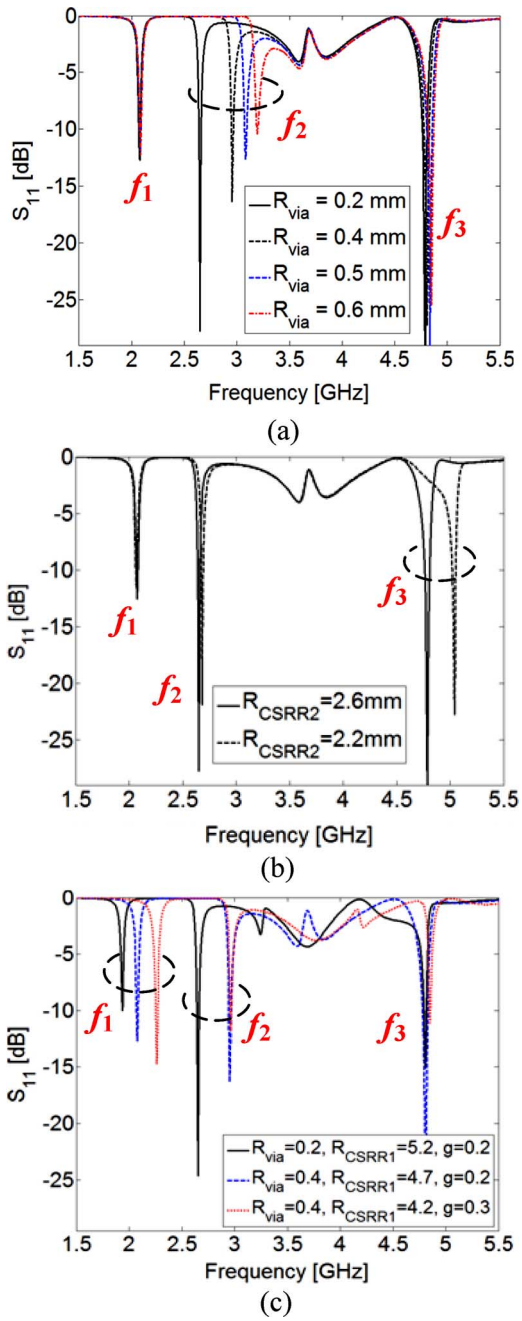

Fig. 2. S_{11} of the proposed MTM antenna versus (a) $\mathrm{R_{via}}$, (b) $\mathrm{R_{CSRR2}}$, (c) $\mathrm{R_{via}}$, $\mathrm{R_{CSRR1}}$, and g.

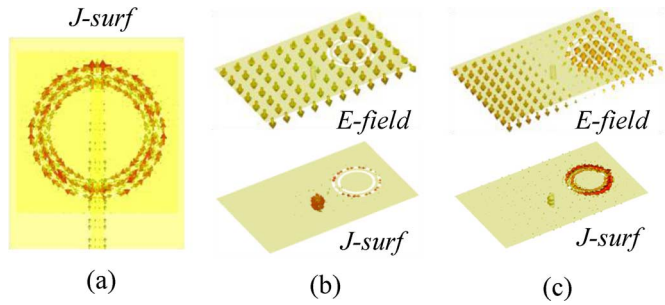

Fig. 3. (a) Surface current distribution on CSRR1 unit at f_1. Electric field and current distribution of mushroom-CSRR2 unit at (b) f_2, and (c) f_3.

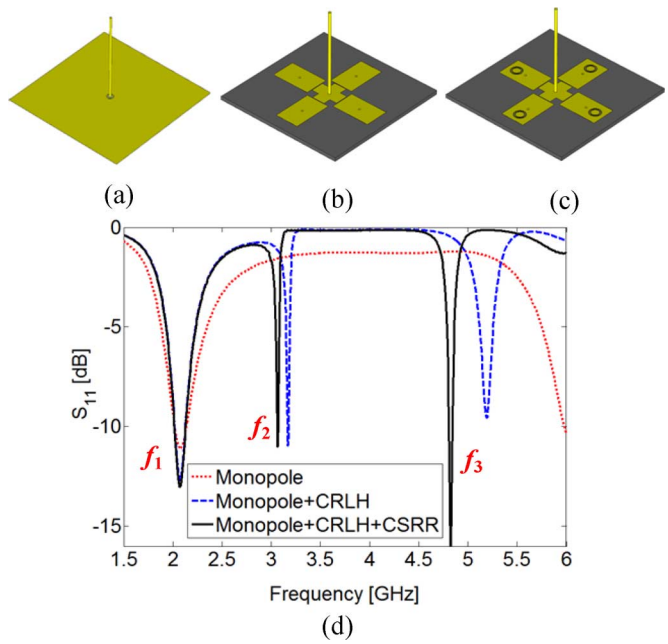

Fig. 4. Monopole wire antenna above ground, (a) unloaded antenna, (b) loaded by CRLH unit ($\mathrm{R_{via}} = 0.5$ mm), (c) loaded by CRLH-CSRR unit, (d) S_{11} parameter.

TABLE I
BANDWIDTH (BW) OF THE ANTENNAS AT RESONANT FREQUENCIES

Antenna type	BW criteria	BW at f_1	BW at f_2	BW at f_3
Wire monopole	S_{11} = -6 dB	255 MHz	28 MHz	65 MHz
	S_{11} = -10 dB	118	10	34
CSRR1monopole	S_{11} = -6 dB	32	50	90
	S_{11} = -10 dB	14	21	52

The -6 and -10 dB bandwidth of the CSRR1 monopole (Fig. 1(a)) and wire monopole (Fig. 4(c)) is given in Table I at resonant frequencies. The f_1, f_2, and f_3 resonant frequencies of both antennas are 2.1, 3.1, and 4.8 GHz, respectively. The proposed antenna shows sufficient bandwidth enough for narrowband vehicular applications.

The normalized radiation pattern of the proposed MTM antenna in Fig. 1(a) is obtained at the E-plane (*xz*) and H-plane (*xy*) as displayed in Fig. 5. It is observed that monopole-shape radiation is obtained over the three frequency bands. Over f_1 frequency band, the z-directed monopole-CSRR1 structure is radiating, as a result, the radiation pattern becomes monopolar. ZOR units resonating at f_2 are known as the radiators with monopole-shape radiation pattern. All patch elements loaded by CSRR2 units resonate over f_3 frequency band radiating $\mathrm{TM_{10}}$ mode. Due to the symmetry, the radiated fields of the out of phase current distributions of $\mathrm{TM_{10}}$ mode cancel out each other in the broadside direction. Therefore, monopolar radiation is achieved at f_3. The radiation efficiency at f_1, f_2, and f_3 are calculated as 26.3, 77.4, and 86.1%, respectively. Low radiation efficiency at f_1 is due to the high level of miniaturization. The via radius affects the efficiency at f_2 so that smaller values of $\mathrm{R_{via}}$ leads to less efficiency due to the increase of ohmic loss in via. Note that the radiator at f_3 frequency is microstrip patch so that the role of CSRR2 is only to couple the power and to

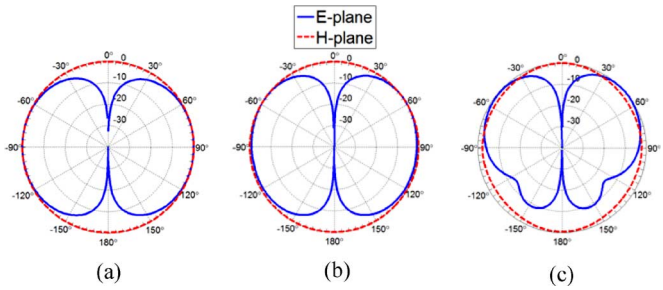

Fig. 5. Normalized radiation pattern at (a) f_1, (b) f_2, and (c) f_3.

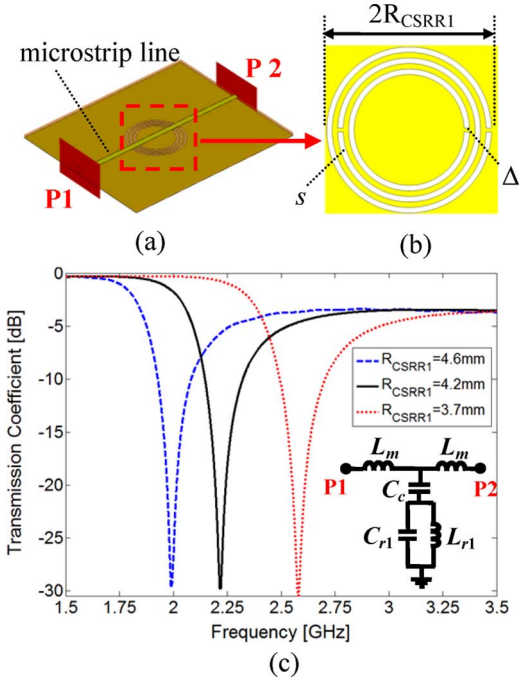

Fig. 6. (a) Two-port microstrip line loaded by CSRR, (b) CSRR structure, (c) transmission coefficient between ports.

adjust the resonant frequency. Hence, the radiation efficiency is quite high over f_3 band.

In order to model and to characterize the used MTM units, several simulation setups were created. Fig. 6 shows the microstrip setup to characterize CSRR structures [23]. For the sake of brevity, only the analysis of CSRR1 is provided. The RO4003 substrate with thickness of 0.5 mm is used. The transmission coefficient between two ports is shown in Fig. 6(c) with circuit model given at inset. CSRR1 unit is modeled by C_{r1}, and L_{r1} resonator tank. The power coupled from the microstrip line to CSRR through C_c capacitance. Changing the radius of CSRR1 affects L_{r1} such that the resonant frequency $f_{r1} = 1/(2\pi\sqrt{L_{r1}(C_c + C_{r1})})$ can be tuned accordingly. Note that the calculated f_r obtained from this setup is very close to the resonant frequency f_1 of the antenna shown in Fig. 2(c). Not shown here, we investigate the effect of the number of slot rings on the resonant frequency since more ring slots reduce f_{r1} [24]. Given $\mathrm{R_{CSRR1}} = 4.2$ mm, it was observed that f_{r1} increases from 2.22 GHz to 2.42 GHz by removing the smallest inner slot. The equivalent circuit parameters of CSRR1 are obtained as $C_c = 1.3$ pF, $C_{r1} = 0.5$ pF, and $L_{r1} = 3.5$ nH.

Two simulation setups are established to characterize mushroom structure as illustrated in Fig. 7. In Fig. 7(a), a unit cell is

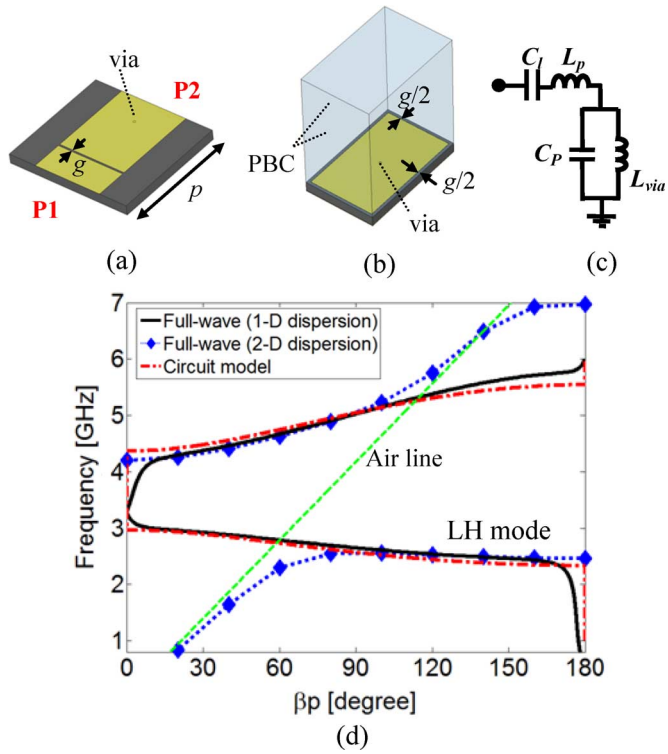

Fig. 7. (a) Two-port simulation setup, (b) eigenmode simulation setup, (c) circuit model, (d) dispersion diagram.

excited at two ports, P1 and P2, to extract the one-dimensional 1-D dispersion diagram using

$$\beta p = \cos^{-1}\left(\frac{1 - S_{11}S_{22} + S_{21}S_{12}}{2S_{21}}\right) \tag{1}$$

where S_{11}, S_{21}, S_{12}, and S_{22} are scattering parameters. The 2-D dispersion diagram is also calculated by exploiting the eigenmode solver using periodic boundary conditions as shown in Fig. 7(b). The equivalent circuit model parameters of the mushroom structure is also extracted and the dispersion diagram is calculated using

$$\beta p = \cos^{-1}\left[1 - 0.5\left(\frac{1}{\omega^2 L_{\mathrm{via}} C_l} + \omega^2 L_p C_p - \frac{L_p}{L_{\mathrm{via}}} - \frac{C_p}{C_l}\right)\right] \tag{2}$$

where $\omega = 2\pi f$. Fig. 7(d) shows that the circuit model predicts the structure frequency response very well. The resonant frequency of zero order mode is $f_r = 1/(2\pi\sqrt{L_{\mathrm{via}}C_p})$. The equivalent parameters are obtained as $C_l = 0.35$ pF, $C_p = 3.2$ pF, $L_{\mathrm{via}} = 0.9$ nH, and $L_p = 3.8$ nH. Using the characterized circuit model of the MTM units, the circuit model of the antenna shown in Fig. 1(a) is developed as illustrated in Fig. 8. The probe feed is represented by L_f inductance. The C_f, L_{p1}, C_e, and L_{p2} elements are used to model the feed section before the gap distance g. The gap distance between the feed section and the mushroom structure is modeled by C_g capacitance. The printed monopole loaded by CSRR1 resonating at f_1 is modeled by L_m, C_c, L_{r1}, C_{r1}, and R_{r1} elements. The ZOR unit, which resonates at f_2, is represented by L_{p3}, R_p, C_p, and L_{via}. The patch radiating at f_3 is modeled by R_A, C_A, L_A tank so that the power

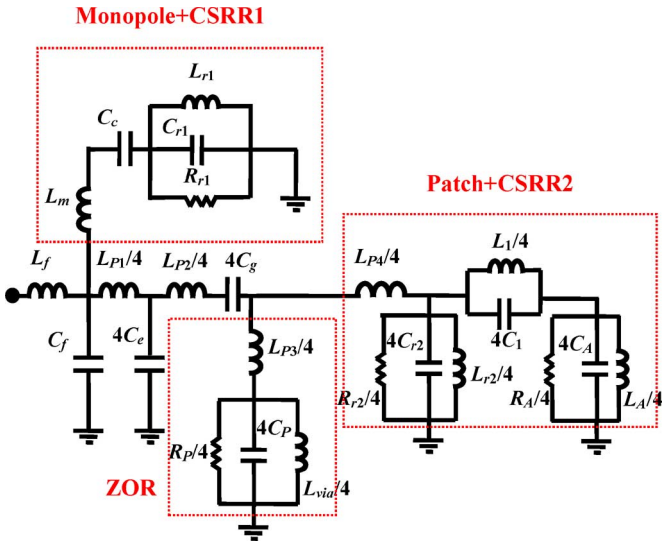

Fig. 8. Equivalent circuit model of the MTM antenna.

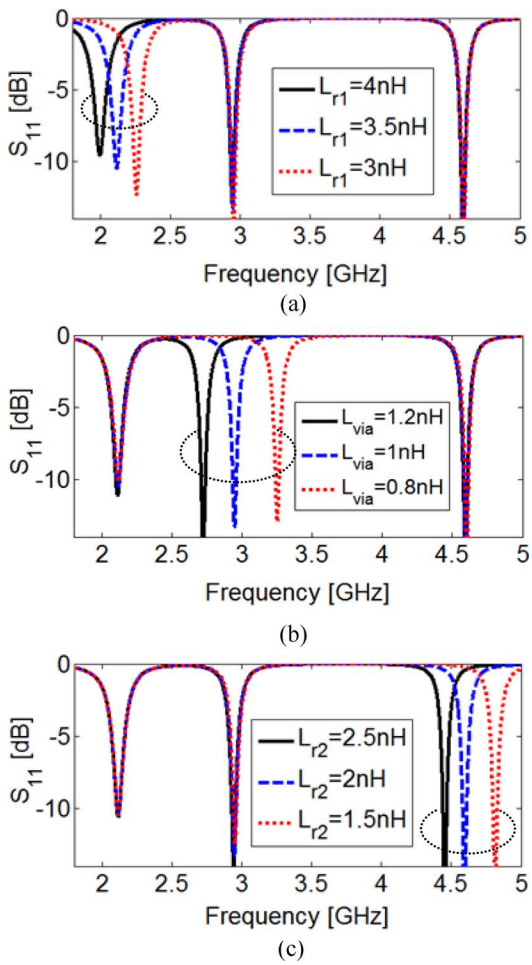

Fig. 9. S_{11} of the circuit model versus (a) L_{r1}, (b) $L_{\rm via}$, and (c) L_{r2} parameters.

is coupled from CSRR2 to patch through L_1-C_1 circuit. The coupling consists of both inductive and capacitive couplings. The factor 4 is applied since four sections are in parallel configuration in the antenna geometry. The circuit model parameters are $L_f = 1.5$ nH, $C_f = 0.5$ pF, $L_m = 0.6$ nH, $C_c = 1.3$ pF, $C_{r1} = 0.5$ pF, $L_{r1} = 3.5$ nH, $R_{r1} = 1500\ \Omega$, $L_{p1} = 1.5$ nH, $C_e = 0.2$ pF, $L_{p2} = 0.2$ nH, $C_g = 0.45$ pF, $L_{p3} = 3.8$ nH, $C_p = 3.2$ pF, $L_{\rm via} = 1$ nH, $R_p = 800\ \Omega$, $L_{p4} = 3.8$ nH, $C_{r2} = 0.4$ pF, $L_{r2} = 2$ nH, $R_{r2} = 1500\ \Omega$, $L_1 = 1.2$ nH, $C_1 = 1.3$ pF, $L_A = 0.2$ nH, $C_A = 1$ pF, and $R_A = 50\ \Omega$. Fig. 9 shows the S_{11} parameter of the circuit model for various L_{r1}, $L_{\rm via}$, and L_{r2} values so that the resonant frequency can be tuned at f_1, f_2, and f_3, by adjusting these parameters independently. It is in agreement with the results shown in Fig. 2 since changing $\rm R_{CSRR1}$, $\rm R_{via}$, and $\rm R_{CSRR2}$ radii affects the L_{r1}, $L_{\rm via}$ and L_{r2} inductances of MTM units, respectively. Note that the circuit model cannot predict two weak resonances between 3.5 and 4 GHz shown in Fig. 2(a) since the circuit components to model higher order modes of printed monopole loaded by CSRR1 are not considered in the circuit model.

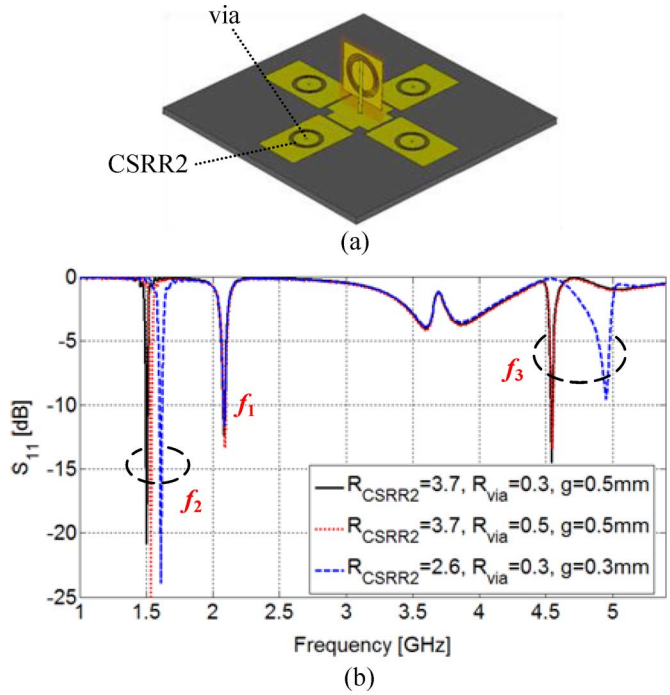

Fig. 10. (a) Proposed MTM antenna with CSRR at the center of mushroom unit, (b) S_{11} parameter.

In [33], it was shown that the LH mode frequency response of a mushroom cell can be reduced by etching CSRR at the center of patch where via is located. In order to achieve further miniaturization at f_2, the CSRR2 unit is shifted to the center of the mushroom patch as illustrated in Fig. 10. It is observed that the resonant frequency f_2 is reduced significantly to about 1.6 GHz. The 1-D dispersion diagram using a two-port simulation setup is calculated as shown in Fig. 11. The LH mode curve is decreased by increasing $\rm R_{CSRR2}$ such that it is reduced by about 1.2 GHz for $\rm R_{CSRR2} = 3.7$ mm. The same reduction of resonant frequency of the antenna is obtained at f_2 so that it is reduced from about 2.8 GHz (see Fig. 2) to 1.6 GHz as shown in Fig. 9(b). In fact, the CSRR inductance and capacitance strongly contributes to the inductance and capacitance of the mushroom structure. However, due to the considerable miniaturization and ohmic loss, the antenna radiation efficiency is reduced to 9.5% at f_2 frequency range. The radiation efficiency at f_1 and f_3 is calculated as 28.1 and 70.8%, respectively. The number of

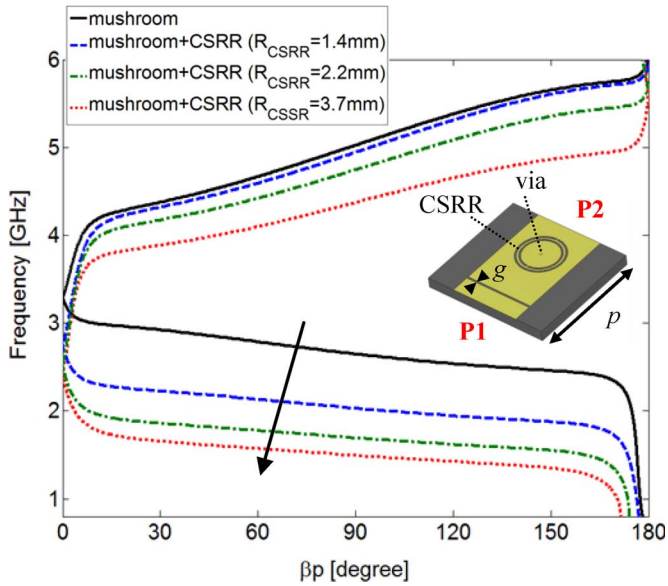

Fig. 11. Dispersion diagram of the mushroom unit cell ($R_{via} = 0.3$ mm) with CSRR at the center.

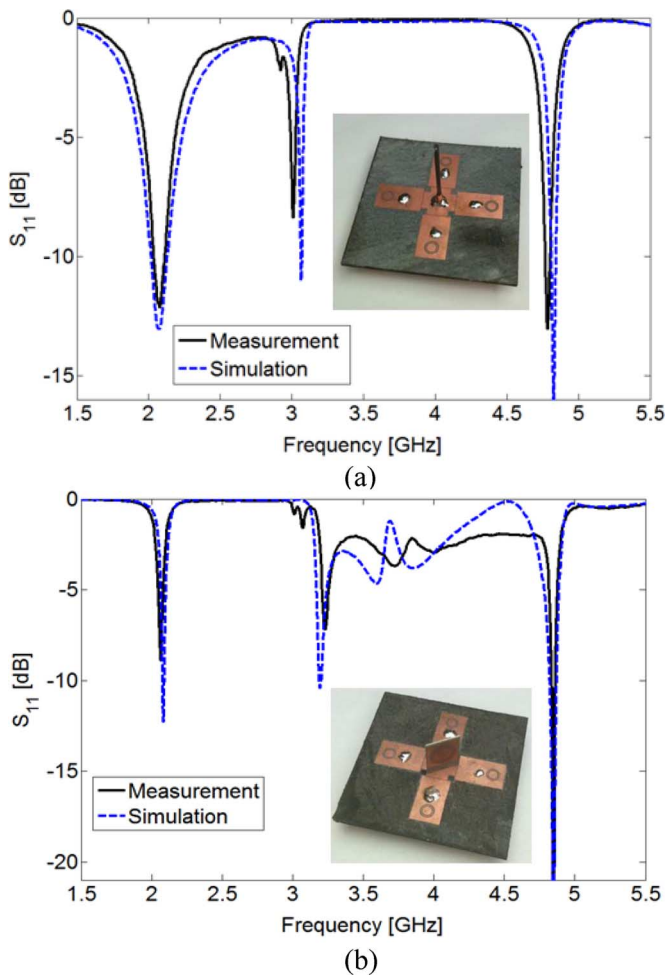

Fig. 12. S_{11} of the MTM antennas, (a) monopole wire with height of 35.5 mm and mushrooms with $R_{via} = 0.5$ mm, (b) printed monopole loaded by CSRR1 structure with $R_{CSRR1} = 4.7$ and mushrooms with $R_{via} = 0.6$ mm.

slot rings has a significant effect on the miniaturization so that we observed that for $R_{CSRR2} = 3.7$ mm, f_2 increases from 1.6 GHz to 2.2 GHz by removing the inner slot.

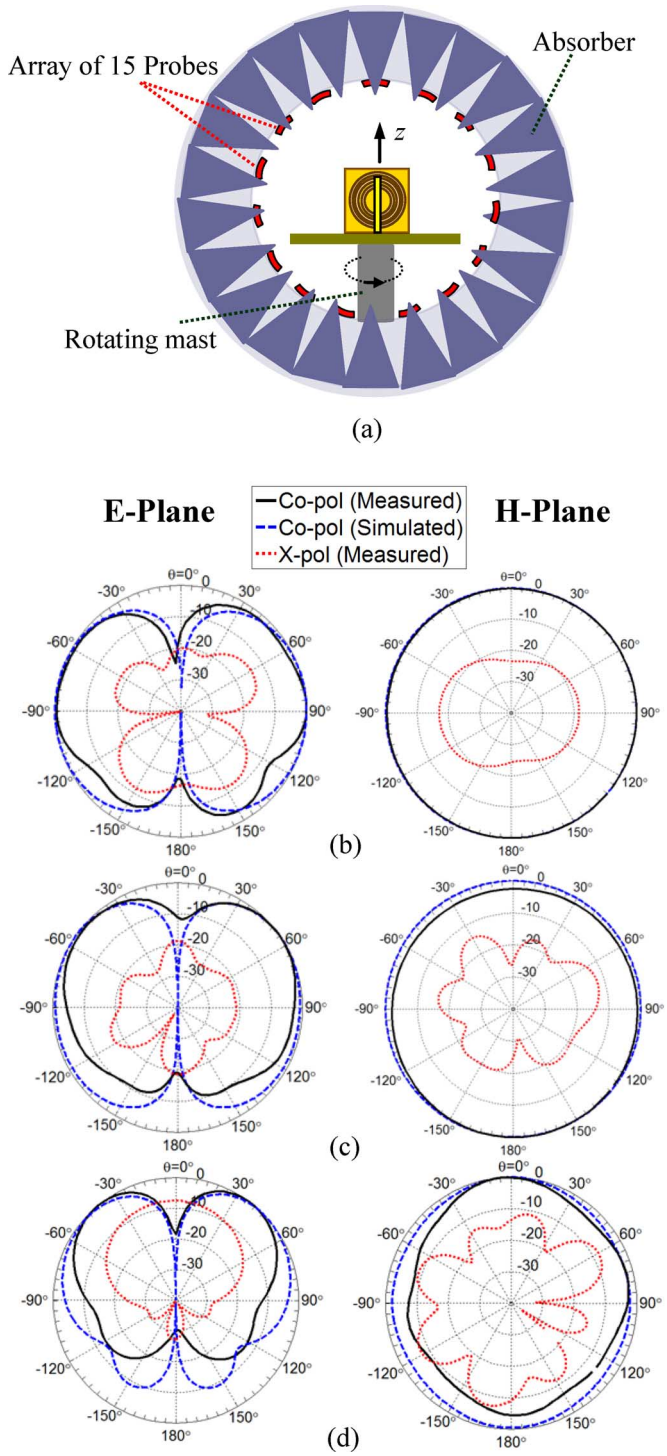

Fig. 13. (a) SATIMO measurement setup. Normalized radiation pattern at E- (xz-) and H- (xy-) planes at (b) f_1, (c) f_2, and (d) f_3 frequencies.

III. Experimental Results

In order to validate simulations, two prototypes are fabricated, one with wire monopole and the second with the printed monopole loaded by CSRR1 unit, as shown in Fig. 12. In both cases the mushroom units are printed on RO5880 substrate with thickness of 1.57 mm and tan $\delta = 0.0009$. The wire monopole diameter is 1.3 mm with the length of 35.5 mm. The radius of via in Fig. 12(a) and (b) is 0.5 and 0.6 mm, respectively. The substrate of printed monopole is RO4003 with thickness of 0.5 mm

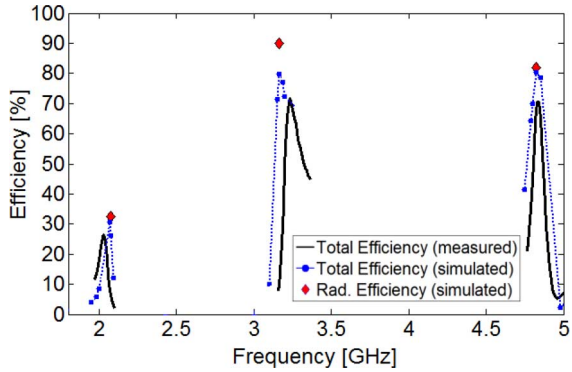

Fig. 14. Radiation efficiency of printed monopole with CSRR1 unit.

TABLE II
REALIZED PEAK GAIN OF THE ANTENNAS

Antenna Type		f_1	f_2	f_3
Wire+CRLH+CSRR2 (Fig. 11a)	Sim.	1.2 dB	0.7	5.6
	Meas.	0.9 dB	0.1	5.2
CSRR1+CRLH+CSRR2 (Fig. 11b)	Sim.	-3.6 dB	1.3	4.7
	Meas.	-4.7 dB	0.5	4.3

and $\tan\delta = 0.0027$. The antennas are fed through a 50-ohm SMA connector from below the ground plane. The rest of geometrical parameters are $\mathrm{R_{CSRR1}} = 4.7, \mathrm{R_{CSRR2}} = 2.6, w_1 = 8, w_2 = 13, d = 4.7, s_1 = s_2 = 0.3, \Delta_1 = \Delta_2 = 0.2, L_1 = 18, L_2 = 11, g = 0.2, w = 0.9, h_m = 13$, and $h_s = 16$ mm. The antennas are fabricated using LPKF laser machine. The reflection coefficient of the antennas is measured using Agilent 8722ES network analyzer. A good agreement is observed between the simulations and measurements. The small discrepancy is due to the imperfection of the fabrication.

As shown in Fig. 13(a), the normalized radiation pattern of the antenna is measured in Starlab SATIMO anechoic chamber with frequency range of 800 MHz to 6 GHz [34]. For the sake of brevity, only the results of printed monopole with CSRR1 unit are reported. Figs. 13(b)–(d) show that the radiation pattern is monopolar at all three operating frequencies. The measured total efficiency, which includes both ohmic loss and mismatch, of the antenna is reported in Fig. 14 and compared well with simulated results at f_1, f_2, and f_3 resonant frequencies. The realized peak gain is measured for two antennas as reported in Table II. The discrepancy between simulated and measured results can be due to the connector loss and mismatch factor. It is observed that via with smaller radius leads to lower radiation efficiency and peak gain at f_2 because of more ohmic loss of via. CSRR1 resonator reduces the antenna gain at f_1 due to the loss and miniaturization compared to the wire monopole antenna. Note that in order to boost the signal strength in vehicular systems, low noise amplifiers (LNAs) might be used at the antenna input to compensate for either low radiation efficiency or signal attenuation caused by long cables between the antenna and receiver [35], [36]. For example, in [35], the reduced radiation efficiency of a rod antenna due to length miniaturization is compensated for by using LNA at the antenna input. In [36], in-line built LNA with gain of 23 dB is used to compensate for the loss caused by long cable feed between a GPS vehicle antenna and the receiver. However, it should be noted that adding LNAs may increase the overall cost of system.

IV. CONCLUSION

Low-profile multiband monopole antennas loaded by mushroom and CSRR metamaterial structures have been proposed. The antennas operate at three tunable frequency bands with monopolar radiation pattern characteristics. Using printed monopole loaded by CSRR1 unit, the height of wire monopole was reduced by 60% with the cost of radiation efficiency. The monopole is loaded in azimuth plane by mushroom units as ZOR. Mushrooms are loaded by CSRR2 units to introduce the third resonant frequency. In this case, the power is coupled through CSRR2 to the rectangular patch to be radiated. By positioning the center of CSRR2 at via location, in addition to the third resonance due to the coupled power to patch, further miniaturization at ZOR frequency of resonance is achieved due to the increase of inductance and capacitance at the shunt arm caused by CSRR2 structure. An equivalent circuit model of the antenna has been proposed which predicts the frequency response very well. A good agreement has been observed between the experimental and simulation results. A multiband tunable frequency response, monopolar radiation pattern characteristics, and miniaturized profile make the proposed antennas a good candidate for vehicular communication systems.

REFERENCES

[1] U. Lee, R. Cheung, and M. Gerla, "Emerging vehicular applications," in *Vehicular Networks: From Theory to Practice*, S. Olario and M. C. Weigle, Eds. Boca Raton, FL, USA: CRC Press, 2009, Ch. 6.
[2] U. Lee, E. Magistretti, B. Zhou, M. Gerla, P. Bellavista, and A. Corradi, "MobEyes: Smart mobs for urban monitoring with vehicular sensor networks," *IEEE Wireless Commun.*, vol. 13, no. 5, pp. 51–57, 2006.
[3] T. M. Fernández-Caramés, M. González-López, and L. Castedo, "Mobile WiMAX for vehicular applications: Performance evaluation and comparison against IEEE 802.11p/a," *Computer Networks (Elsevier)*, vol. 55, no. 16, pp. 3784–3795, 2011.
[4] G. Zaggoulos, A. Nix, and A. Doufexi, "WIMAX system performance in highly mobile scenarios with directional antennas," presented at the IEEE Personal, Indoor and Mobile Radio Commu. Symp. (PIMRC'07), Athens, Greece, 2007.
[5] C. F. Mecklenbrauker, A. F. Molisch, J. Karedal, F. Tufvesson, A. Paier, L. Bernado, T. Zemen, O. Klemp, and N. Czink, "Vehicular channel characterization and its implications for wireless system design and performance," *Proc. IEEE*, vol. 99, no. 7, pp. 1189–1212, 2011.
[6] P. L. Werner and D. H. Werner, "Design synthesis of miniature multiband monopole antennas with application to ground-based and vehicular communication systems," *IEEE Antennas Wireless Propag. Lett.*, vol. 4, pp. 104–106, 2005.
[7] D. Ribbenfjärd, B. Lindmark, B. Karlsson, and L. Eklund, "Omnidirectional vehicle antenna for measurement of radio coverage at 2 GHz v.2.0," *IEEE Antennas Wireless Propag. Lett.*, vol. 3, pp. 269–272, 2004.
[8] I. Sen and D. W. Matolak, "Vehicle—Vehicle channel models for the 5-GHz band," *IEEE Trans. Intell. Transp. Syst.*, vol. 9, no. 2, pp. 235–245, 2008.
[9] H. T. Cheng, H. Shan, and W. Zhuang, "Infotainment and road safety service support in vehicular networking: From a communication perspective," *Mech. Syst. Signal Process.*, vol. 25, no. 6, pp. 2020–2038, 2011.
[10] T. L. Doumi, "Spectrum considerations for public safety in the United States," *IEEE Commun. Mag.*, vol. 44, no. 1, pp. 30–37, 2006.
[11] S. R. Best, "On the resonant properties of the Koch fractal and other wire monopole antennas," *IEEE Antennas Wireless Propag. Lett.*, vol. 1, pp. 74–76, 2002.
[12] B. Ghosh, S. K. M. Haque, D. Mitra, and S. Ghosh, "A loop loading technique for the miniaturization of non-planar and planar antennas," *IEEE Trans. Antenna Propag.*, vol. 58, no. 6, pp. 2116–2121, 2012.

[13] Y. Dong and T. Itoh, "Metamaterial-based antennas," *Proc. IEEE*, vol. 100, no. 7, pp. 2271–2285, 2012.
[14] J. Q. Gong, J. B. Jiang, and C. H. Liang, "Low-profile folded-monopole antenna with unbalanced composite right-/left-handed transmission line," *Electron. Lett.*, vol. 48, no. 14, pp. 813–815, 2012.
[15] H. Iizuka and P. S. Hall, "Left-handed dipole antennas and their implementations," *IEEE Trans. Antennas Propag.*, vol. 55, no. 5, pp. 1246–1253, 2007.
[16] G. V. Eleftheriades, A. Grbic, and M. Antoniades, "Negative-refractive-index metamaterials and enabling electromagnetic applications," in *Proc. IEEE Antennas Propag. Soc. Symp.*, Jun. 2004, vol. 2, pp. 1399–1402.
[17] A. Sanada, M. Kimura, I. Awai, C. Caloz, and T. Itoh, "A planar zeroth order resonator antenna using a left-handed transmission line," in *Proc. EuMC*, 2004, pp. 1341–1344.
[18] J. Zhu and G. V. Eleftheriades, "A compact transmission-line metamaterial antenna with extended bandwidth," *IEEE Antennas Wireless Propag. Lett.*, vol. 8, pp. 295–298, 2009.
[19] F. J. Herraiz-Martínez, P. S. Hall, Q. Liu, and D. Segovia-Vargas, "Left-Handed wire antennas over ground plane with wideband tuning," *IEEE Trans. Antenna Propag.*, vol. 59, no. 5, pp. 1460–1471, 2011.
[20] A. A. Ibrahim and A. M. E. Safwat, "Microstrip-fed monopole antennas loaded with CRLH unit cells," *IEEE Trans. Antenna Propag.*, vol. 60, no. 9, pp. 4027–4036, 2012.
[21] S.-T. Ko and J.-H. Lee, "Broad E-plane beamwidth zeroth-order resonance patch antennaa," in *Proc. IEEE Antennas Propag. Soc. Symp.*, 2012, pp. 5431–5434.
[22] J. Zhu and G. V. Eleftheriades, "Dual-band metamaterial-inspired small monopole antenna for WiFi applications," *Electron. Lett.*, vol. 45, no. 22, 2009.
[23] J. D. Baena, J. Bonache, F. Martín, R. M. Sillero, F. Falcone, T. Lopetegi, M. A. G. Laso, J. García-García, I. Gil, M. F. Portillo, and M. Sorolla, "Equivalent-circuit models for split-ring resonators and complementary split-ring resonators coupled to planar transmission lines," *IEEE Trans. Microw. Theory Tech.*, vol. 53, no. 4, pp. 1451–1461, 2005.
[24] F. Bilotti, A. Toscano, and L. Vegni, "Design of spiral and multiple split-ring resonators for the realization of miniaturized metamaterial samples," *IEEE Trans. Antennas Propag.*, vol. 55, no. 8, pp. 2258–2267, 2007.
[25] Ó. Quevedo-Teruel, M. N. M. Kehn, and E. Rajo-Iglesias, "Dual-band patch antennas based on short-circuited split ring resonators," *IEEE Trans. Antenna Propag.*, vol. 59, no. 8, pp. 2758–2765, 2011.
[26] Y. Lee, S. Tse, Y. Hao, and C. G. Parini, "A compact microstrip antenna with improved bandwidth using complementary split-ring resonator (CSRR) loading," in *Proc. IEEE Antennas Propag. Soc. Symp.*, 2007, pp. 5431–5434.
[27] O. S. Kim and O. Breinbjerg, "Miniaturised self-resonant split-ring resonator antenna," *Electron. Lett.*, vol. 45, no. 4, pp. 196–197, 2009.
[28] R. O. Ouedraogo, E. J. Rothwell, A. R. Diaz, K. Fuchi, and A. Temme, "Miniaturization of patch antennas using a metamaterial-inspired technique," *IEEE Trans. Antennas Propag.*, vol. 60, no. 5, pp. 2175–2182, 2012.
[29] M. S. Sharawi, M. U. Khan, A. B. Numan, and D. N. Aloi, "A CSRR loaded MIMO antenna system for ISM band operation," *IEEE Trans. Antenna Propag.*, vol. 61, no. 8, pp. 4265–4274, 2013.
[30] Y. Dong, H. Toyao, and T. Itoh, "Design and characterization of miniaturized patch antennas loaded with complementary split-ring resonators," *IEEE Trans. Antennas Propag.*, vol. 60, no. 2, pp. 772–785, 2012.
[31] M. Selvanayagam and G. V. Eleftheriades, "A compact printed antenna with an embedded double-tuned metamaterial matching network," *IEEE Trans. Antenna Propag.*, vol. 58, no. 7, pp. 2354–2361, 2010.
[32] CST—Microwave Studio Computer Simulation Technology, 2012.
[33] L. Peng, C.-L. Ruan, and Z.-Q. Li, "A novel compact and polarization-dependent mushroom-type EBG using CSRR for dual/triple-band applications," *IEEE Microw. Wireless Compon. Lett.*, vol. 20, no. 9, pp. 489–491, 2010.
[34] SATIMO—Microwave Vision Group France [Online]. Available: http://www.satimo.com
[35] M. Cerretelli and G. B. Gentili, "Progress in compact multifunction automotive antennas," in *Proc. Int. Conf. Electromagnetics in Advanced Applications*, 2007, pp. 93–96.
[36] GPS Vehicle Antenna (E1215). Espoo, Finland [Online]. Available: http://www.cojot.com/wideband-antennas/vehicle, COJOT Oy, Available:

Aidin Mehdipour (S'07–M'11) received the B.S. degree from Amirkabir University of Technology, Tehran, Iran, in 2003, the M.S. degree from the University of Tehran, Tehran, Iran, in 2006, and the Ph.D. degree from Concordia University, Montreal, QC, Canada, in 2011, all in electrical engineering.

From December 2011 to May 2013, he was a Postdoctoral Fellow at INRS, Montreal, QC, Canada, working on carbon nanocomposites, metamaterial and reconfigurable antennas. Currently he is a Postdoctoral Fellow at the University of Toronto, Toronto, ON, Canada, working on the development of metamaterial leaky-wave antennas for wireless communications. His main research interests include metamaterial structures, small antennas, engineered nanomaterials, leaky-wave antennas, beam steering techniques, RFID, ultrawideband, millimeter wave antennas and microwave circuits.

Dr. Mehdipour is a recipient of Natural Sciences and Engineering Research Council of Canada (NSERC) Postdoctoral Fellowship (2012–2014). He is a winner of Governor General of Canada's Gold Medal in 2011, and the Distinguished Doctoral Dissertation Prize awarded by Concordia University in 2012. He received David J. Azrieli Graduate Fellowship, as the highest ranking Fellowship Award in Concordia University in 2010. He is a member of the IEEE Antennas and Propagation Society, IEEE EMC Society, and the Applied Computational Electromagnetics Society.

Tayeb A. Denidni (M'98–SM'04) received M.Sc. and Ph.D. degrees in electrical engineering from Laval University, Quebec City, QC, Canada, in 1990 and 1994, respectively.

From 1994 to 2000, he was a Professor with the engineering department, Université du Quebec in Rimouski (UQAR), Rimouski, QC, Canada, where he founded the Telecommunications laboratory. Since August 2000, he has been with the Institut National de la Recherche Scientifique (INRS), Université du Quebec, Montreal, QC, Canada. He found RF laboratory at INRS-EM, Montreal. He has a great experience with antenna design and he is leading a large research group consisting of three research scientists, six Ph.D. students, and one M.Sc. student. He served as a principal investigator on many research project sponsored By NSERC, FCI and numerous industries. His current research areas of interest include reconfigurable antennas using EBG and FSS structures, dielectric resonator antennas, metamaterial antennas, adaptive arrays, switched multi-beam antenna arrays, ultra-wideband antennas, microwave and development for wireless communications systems.

From 2008 to 2010, Dr. Denidni served as an Associate Editor for IEEE TRANSACTIONS ON ANTENNAS PROPAGATION. From 2005 to 2007, Dr. Denidni served as an Associate Editor for IEEE Antennas Wireless Propagation Letters. Since 2004, he has been elevated to the grade of Senior Member of the IEEE. In 2012 and 2013, he was awarded by INRS for outstanding research and teaching achievements.

Abdel Sebak (F'10) received the B.Sc. degree from Cairo University, Cairo, Egypt, and the M.Eng. and Ph.D. degrees from the University of Manitoba, MB, Canada, all in electrical engineering.

From 1984 to 1986, he was with the Canadian Marconi Company working on the design of microstrip phased array antennas. From 1987 to 2002, he was a Professor in the ECE Department, University of Manitoba. He is a Professor of Electrical and Computer Engineering, Concordia University, Montreal, QC, Canada. His current research interests include phased array antennas, mm-wave antennas and imaging, computational electromagnetics, and interaction of EM waves with engineered materials and bio-electromagnetics.

Dr. Sebak received the 2000 and 1992 University of Manitoba Merit Award for outstanding Teaching and Research, the 1994 Rh Award for Outstanding Contributions to Scholarship and Research, and the 1996 Faculty of Engineering Superior Academic Performance. Dr. Sebak has served as the Chair for the IEEE Canada Awards and Recognition Committee (2002–2004) and as the Technical Program Chair for the 2002 IEEE CCECE Conference and the 2006 URSI-ANTEM Symposium. Dr. Sebak is the Technical Program Co-Chair for the 2015 IEEE ICUWB Conference. He is a member of the Canadian National Committee of International Union of Radio Science (URSI) Commission B.